THE JOURNAL OF
PHYSICAL CHEMISTRY A

Article

pubs.acs.org/JPCA

Experimental and Theoretical Understanding of the Gas Phase Oxidation of Atmospheric Amides with OH Radicals: Kinetics, Products, and Mechanisms

Nadine Borduas,[†] Gabriel da Silva,[‡] Jennifer G. Murphy,*[,†] and Jonathan P. D. Abbatt*[,†]

[†]Department of Chemistry, University of Toronto, 80 St. George Street, Toronto, Ontario M5S 3H6, Canada

[‡]Department of Chemical and Biomolecular Engineering, The University of Melbourne, Victoria 3010, Australia

S *Supporting Information*

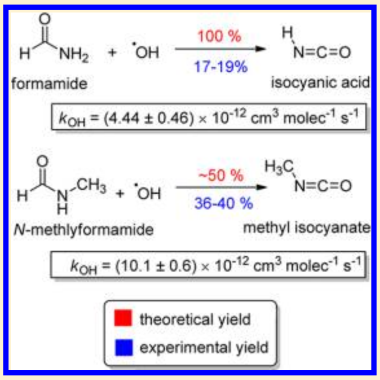

ABSTRACT: Atmospheric amides have primary and secondary sources and are present in ambient air at low pptv levels. To better assess the fate of amides in the atmosphere, the room temperature (298 ± 3 K) rate coefficients of five different amides with OH radicals were determined in a 1 m^3 smog chamber using online proton-transfer-reaction mass spectrometry (PTR-MS). Formamide, the simplest amide, has a rate coefficient of $(4.44 \pm 0.46) \times 10^{-12}$ cm^3 $molec^{-1}$ s^{-1} against OH, translating to an atmospheric lifetime of ~1 day. *N*-methylformamide, *N*-methylacetamide and propanamide, alkyl versions of formamide, have rate coefficients of $(10.1 \pm 0.6) \times 10^{-12}$, $(5.42 \pm 0.19) \times 10^{-12}$, and $(1.78 \pm 0.43) \times 10^{-12}$ cm^3 $molec^{-1}$ s^{-1}, respectively. Acetamide was also investigated, but due to its slow oxidation kinetics, we report a range of $(0.4-1.1) \times 10^{-12}$ cm^3 $molec^{-1}$ s^{-1} for its rate coefficient with OH radicals. Oxidation products were monitored and quantified and their time traces were fitted using a simple kinetic box model. To further probe the mechanism, ab initio calculations are used to identify the initial radical products of the amide reactions with OH. Our results indicate that N−H abstractions are negligible in all cases, in contrast to what is predicted by structure−activity relationships. Instead, the reactions proceed via C−H abstraction from alkyl groups and from formyl C(O)−H bonds when available. The latter process leads to radicals that can readily react with O_2 to form isocyanates, explaining the detection of toxic compounds such as isocyanic acid (HNCO) and methyl isocyanate (CH_3NCO). These contaminants of significant interest are primary oxidation products in the photochemical oxidation of formamide and *N*-methylformamide, respectively.

■ INTRODUCTION

Amides are emitted directly to the atmosphere from biological sources as well as from industrial processes and are present at pptv levels in the atmosphere.[1] In particular, tobacco smoke is a source of formamide, acetamide, and propanamide, presumably formed during the combustion process.[2] Mixing ratios of over 400 pptv of *N*,*N*-dimethylformamide have been observed near waste and sewage operations and an emission rate of 10 mg/kg of *N*,*N*-dibutylformamide has been measured from charbroiling hamburgers.[3,4] *N*,*N*-Dimethylformamide has also been detected from textile floor coverings from a polyamide composite.[5] Amides have been detected in ambient particles, biomass burning aerosols and fogwater, as well.[6−8]

Amides have secondary as well as primary sources to the atmosphere. For example, they can be formed via amine oxidation by OH radicals. Since amines also have biogenic and anthropogenic sources to the atmosphere, including their use in large quantities in carbon capture and storage (CCS) technology, they may represent a significant source of amides to ambient air.[9] This secondary source is of particular concern since amides are typically longer-lived species than amines.[9] Indeed, a recent report by Zhu et al. detected formamide, potentially from amine oxidation, from an industrial scale carbon capture facility in Norway.[10] The mechanism of gas-phase oxidation of amines to amides has also been investigated through ab initio calculations.[11,12]

Only a few studies have looked at the atmospheric fate of amides. Chakir and co-workers measured the cross-section of *N*,*N*-dialkylated amides and determined that its value was smaller than or equal to 3×10^{-20} cm^2 $molec^{-1}$ beyond 270 nm, indicating that photolysis is a negligible sink for amides.[13] Koch et al. were the first to report rate coefficients for the reaction of OH radicals with amides, and they specifically looked at *N*-alkylated acetamides and propanamides, determining values between 5 and 14×10^{-12} cm^3 $molec^{-1}$ s^{-1}.[14] 1-Methyl-2-pyrrolidinone, 2-chloro-*N*-isopropylacetanilide, and *N*-ethylperfluorobutyramide have been the subject of atmospheric fate studies where rate coefficients with OH and NO_3 radicals and with ozone were reported; OH reactivity was found to dominate the fate of these amides.[15−17] Solignac et al. studied the kinetics of OH and Cl radicals with *N*-alkylated

Special Issue: Mario Molina Festschrift

Received: April 16, 2014
Revised: July 11, 2014

dx.doi.org/10.1021/jp503759f | *J. Phys. Chem. A* XXXX, XXX, XXX−XXX

formamides and acetamides and later determined the rate coefficients of OH radicals with cyclic amides.[18,19] In addition, Barnes et al. reviewed these results and completed a product study of the smaller amides, identifying isocyanates as potential oxidation products.[20] NO_3 radicals react with *N*,*N*-dimethylated amides with rate coefficients on the order of 10^{-14} cm^3 $molec^{-1}$ s^{-1}, making the sink of amides toward NO_3 radicals competitive with OH radicals only at night.[21] These kinetics studies have been recently reviewed by Nielsen et al. in the context of the impact of amines on CCS.[9] Furthermore, amides may partition to aerosols but whether this sink is competitive with gas phase oxidation is unknown.

Despite the work summarized above, the atmospheric behavior and reactivity of formamide, the smallest and most volatile of amides, has yet to be investigated. To address this gap, five different amides, (i) formamide, (ii) *N*-methylformamide, (iii) acetamide, (iv) *N*-methylacetamide, and (v) propanamide, were investigated to elucidate their reactivity trends toward the OH radical, their atmospheric lifetimes and ultimately their atmospheric fate. Relative rate coefficients were measured in a smog chamber using online mass spectrometry and the oxidation products' traces were fitted using simple box model kinetics. The mechanism was further evaluated using ab initio calculations to determine the location of the H-abstraction and fate of the resultant radicals.

■ EXPERIMENTAL AND THEORETICAL METHODS

1. Laboratory Study. The relative rate kinetics of five amides were measured using a previously described experimental setup.[22] Briefly, a proton-transfer-reaction mass spectrometer (PTR-MS) (Ionicon Analytik GmbH, Innsbruck Austria)[23] was connected to a 1 m^3 Teflon FEP film (American Durafilm) bag (Ingeniven) mounted on a Teflon-coated frame, surrounded by a total of 12 UVB lamps (Microlites Scientific). The chamber did not contain a fan. The PTR-MS was connected to the chamber by a ~1 m long 1/16″ ID silcocoated steel inlet (Ionicon's standard transfer line) heated to 50 °C linked to an FEP tubing that sampled from the middle of the chamber. The flow through the inlet of the PTR-MS was 100 sccm. These inlet conditions are similar to conditions optimized by Gylestam et al. for the detection of isocyanates by PTR-MS.[24] The signals of the compounds of interest were normalized to m/z 21 corresponding to the $H_3{}^{18}O^+$ ion.

The amides were purchased from Sigma-Aldrich and used as is. The amide calibrations on the PTR-MS were accomplished by injecting known amounts of an aqueous solution of the analyte into a glass tube connected to the chamber. A flow of pure air passed through the glass tube adding the amide to the chamber and resulting in mixing ratios ranging from 40 to 300 ppbv. Amides were all monitored at their respective protonated molecular ion m/z and all had linear calibrations with sensitivities ranging from 14 to 18 ncps/ppbv (see Table S1 and Equation S1).

A typical oxidation experiment consisted of injecting a known amount of an aqueous solution of amide into the dark 1 m^3 chamber. *n*-Butanol was added as the reference compound and detected by the PTR-MS at m/z 57, corresponding to the loss of water from the protonated molecular ion. Compared to amines,[22] amides were better behaved in the smog chamber; little to no conditioning of the walls was required and the amides were detected by the PTR-MS with quick response times. Stable amide signals could also be monitored for hours, further demonstrating their stability within the experimental setup and on the time scale of the oxidation experiment. Most amides, with the exception of acetamide, experienced no decay under lit conditions, in the absence of hydrogen peroxide and on the time scale of the oxidation experiments. Following the establishment of a stable amide signal inside the chamber, pure air from an AADCO 737-series generator was bubbled through an aqueous solution of 30% hydrogen peroxide at a rate of 500 sccm. Approximately 15 min later, the UVB lights surrounding the chamber were turned on to generate OH radicals in concentrations of approximately 2×10^7 molecules cm^{-3}, inferred from the loss rate of *n*-butanol. Hydrogen peroxide was continuously added to the chamber to keep the supply of OH radical precursor approximately constant during the experiment. Experiments were conducted under dry (<1% RH) and NO_x-free conditions.

HNCO was detected as an oxidation product and was quantified using PTR-MS (detected at m/z 44), ion chromatography (IC), and a homemade HNCO source. A flow of HNCO was generated by heating cyanuric acid inside a stainless steel tube to 250 °C, controlled by a thermocouple, while passing a flow of 200 sccm of nitrogen over the headspace of the tube. A dilution flow was added to the headspace flow to avoid high gas-phase concentrations of HNCO and, thus, polymerization of HNCO in the tubing. The source showed variability in its HNCO permeation rate from week to week, so the PTR-MS was independently calibrated by bubbling HNCO through bubblers filled with deionized water at a known rate and for a known amount of time and quantified by IC (see Figure S1). Further experimental details are available in the Supporting Information. We ruled out any interference from $CO_2{}^+$ (also detected at m/z 44), since ambient CO_2 concentrations of ~380 ppmv do not produce any significant signal at m/z 44 in the PTR-MS. Control experiments involving H_2O_2 and UVB light, but in the absence of a gas-phase amide, showed production of HNCO, implying a background signal for this weak acid in the chamber. This background was accounted for in the yield calculation by averaging the final HNCO signal of more than 10 control experiments and subtracting this value (ranging from 8 to 40% of the total signal) from the final HNCO signal in the amide oxidation experiments. The yield reported is the quotient of moles of product produced (corrected by its respective background signal) divided by the moles of amide that decayed away at the end of the reaction, that is, when the lights surrounding the chamber were turned off. This method of calculating yields was verified by plotting the appearance of product versus the loss of starting material and taking the slope of that plot as the yield as well as verified by the kinetic model fits. The yields reported represent the range measured during different experiments.

Methyl isocyanate was also detected as an oxidation product at m/z 58. To correct for its decay, the methyl isocyanate time trace was subtracted by 4% of the *n*-butanol signal at m/z 57, a percentage that represents the natural abundance of ^{13}C in *n*-butanol, which has an isobaric interference with methyl isocyanate. Formamide (m/z 46) was corrected by subtracting 2% of the acetaldehyde signal at m/z 45 to account for its ^{13}C contribution to m/z 46.

Following each oxidation experiment, the chamber was purged at least overnight with pure air. The chamber was also cleaned on a weekly basis by bubbling 30% hydrogen peroxide into an amide-free chamber with the UVB lights turned on for several hours. A small background signal of formamide and HNCO was observed during these control experiments,

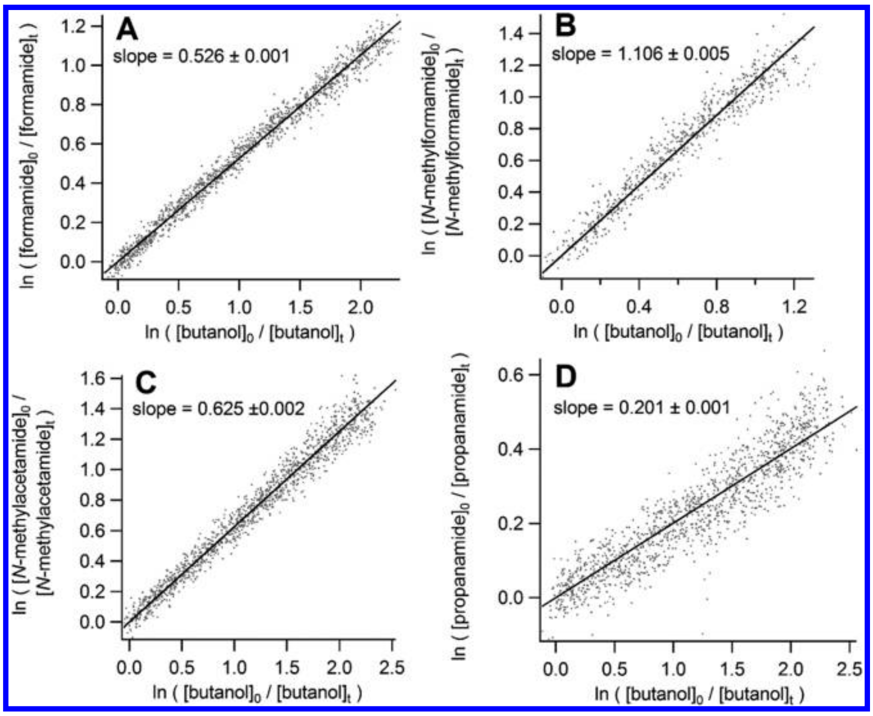

Figure 1. Plot of eq 1 for formamide (A), *N*-methylformamide (B), *N*-methylacetamide (C), and propanamide (D), where the linear regression is forced through the origin.

suggesting a contribution of wall chemistry within this experimental set up. The product yields reported have been corrected using these background signals.

2. Ab Initio Study. The mechanism of OH radicals reacting with the five studied amides, as well as the reaction of select product radicals with O_2, was investigated using computational ab initio methods. Structures were optimized using the M06-2X density functional with the 6-31G(2df,p) basis set.[25] Subsequent higher-level energies were obtained using the G3X-K composite theoretical method.[26] This method has been designed specifically for accurate thermochemical kinetics, and utilizes the M06-2X/6-31G(2df,p) structures in a series of single point energy calculations with basis sets of incrementally decreasing size, from Hartree–Fock theory to perturbation theory (MP2, MP3, MP4) and, ultimately, to coupled cluster theory (CCSD(T)). Energies calculated at these levels are combined with empirical scaling terms to arrive at the final G3X-K energy. Energies quoted here are 0 K enthalpies (i.e., electronic energy + zero point energy) and are expected to be accurate to within 1 kcal mol^{-1} on average.[26] All calculations were performed using the Gaussian 09 code.[27]

■ RESULTS AND DISCUSSION

1. Kinetics Results. Upon exposure to OH radicals inside the 1 m^3 smog chamber, the amides under study exhibited pseudo-first order decay kinetics at room temperature (298 ± 3 K) and atmospheric pressure. The relative rate method[28] allowed for the determination of their respective bimolecular rate coefficients using *n*-butanol as the reference compound. Accurate knowledge of the rate coefficient of *n*-butanol with OH radicals, (8.86 ± 0.85) × 10^{-12} cm^3 molec^{-1} s^{-1}, is necessary to employ eq 1.[29] A plot of the natural logarithm of the normalized amide decay signal as a function of the natural logarithm of the normalized *n*-butanol decay signal yields the ratio of both rate coefficients, $k_{\text{amide+OH}}/k_{\text{butanol+OH}}$ (Figure 1A–D). Note that *n*-butanol serves as a good reference compound as it does not react with amides, has no observable wall loss, and is detected at *m*/*z* 57 by the PTR-MS, which does not interfere with other signals of interest.

Rate coefficients were determined based on a minimum of three reproducible experiments for formamide (4.44 ± 0.46) × 10^{-12} cm^3 molec^{-1} s^{-1}, *N*-methylformamide (10.1 ± 0.6) × 10^{-12} cm^3 molec^{-1} s^{-1}, *N*-methylacetamide (5.42 ± 0.19) × 10^{-12} cm^3 molec^{-1} s^{-1}, and propanamide (1.78 ± 0.43) × 10^{-12} cm^3 molec^{-1} s^{-1}. See Figure 1A–D, for typical relative rate plots for the four amides studied. Furthermore, forcing the linear regression through the origin does not change the slope by more than 5%, a value consistently less than the reported standard deviation of the experiments.

Barnes et al. used an FTIR technique to study the kinetics of other amides but reported interference in the method when looking at formamide.[20] Consequently, this study represents the first reported experimental rate coefficient for formamide and compares well with Barnes' predicted value of 4 × 10^{-12} cm^3 molec^{-1} s^{-1}. In addition, our value for *N*-methylformamide lies within the uncertainty of Barnes et al.'s value of (8.6 ± 2.4) × 10^{-12} cm^3 molec^{-1} s^{-1}.[20] *N*-Methylacetamide's reaction with OH radicals has been previously investigated, once by Koch et al., (5.2 ± 0.19) × 10^{-12} cm^3 molec^{-1} s^{-1}, and again by Barnes et al., (11 ± 3) × 10^{-12} cm^3 molec^{-1} s^{-1}.[14,20] The value obtained in this relative rate study closely matches Koch et al.'s value, measured by absolute rate kinetics using flash photolysis coupled to resonance fluorescence. This study is also the first to report the rate coefficient of propanamide with OH radicals. Since its rate coefficient is significantly slower than the reference compound, a slightly more scattered rate plot was observed (Figure 1D).

The uncertainty reported with the rate coefficients represents the standard deviation of multiple experiments and is less than a 10% error for formamide, *N*-methylformamide, and *N*-

methylacetamide. An additional uncertainty arises from the rate coefficient of the reference compound *n*-butanol with OH radicals, and consequently, a total uncertainty closer to 20% should be considered when using these rate coefficients in model evaluations. Propanamide's rate coefficient is approximately five times slower than the reference compound *n*-butanol, which leads to an uncertainty of 24%.

Acetamide was also investigated under identical conditions but since its oxidative decay was difficult to reproduce, in part due to a slow reaction and an unsteady signal inside the chamber, a large uncertainty on the rate coefficient was obtained. Based on three experiments, an average rate coefficient of $(0.77 \pm 0.35) \times 10^{-12}$ cm^3 molec^{-1} s^{-1} was measured for acetamide (see Figure S3 for a typical plot). The previously published value by Barnes et al. of $(3.5 \pm 1.0) \times 10^{-12}$ cm^3 molec^{-1} s^{-1} is quite high compared to our experimental results.[20] We choose to report a range of (0.4−1.1) × 10^{-12} cm^3 molec^{-1} s^{-1} for acetamide to take into consideration the large uncertainty associated with this measurement.

$$\ln\left(\frac{[\text{amide}]_0}{[\text{amide}]_t}\right) = \frac{k_{\text{amide+OH}}}{k_{\text{butanol+OH}}}\ln\left(\frac{[\text{butanol}]_0}{[\text{butanol}]_t}\right) \tag{1}$$

2. Reaction Products and Mechanisms. The experimental decays of formamide, *N*-methylformamide, *N*-methylacetamide, and propanamide, and the production of their respective oxidation products were fitted using simple kinetic box model equations (see Supporting Information for full description of equations). The yields of the oxidation products were also quantified (see Scheme 1). Because the reaction of acetamide was slower, we were unable to reproducibly quantify the yields of its oxidation products. HNCO was detected under all experimental conditions as a primary product from formamide and possibly as a primary or secondary product from the other amides investigated. HNCO is toxic through protein carbamylation and so exposure levels through biomass burning and diesel exhaust are currently of concern.[30,31] A recent report evaluating HNCO concentrations at three different urban and regional sites in the U.S. found mixing ratios ranging from <0.003 to 1.2 ppbv and suggest the presence of both primary and secondary sources to explain observed diurnal profiles.[32]

Scheme 1. Product Identification and Quantification of Amide Oxidation by OH Radicals in a 1 m^3 Teflon FEP Film Bag and in the Absence of NO$_x$ Based on Experimental and Theoretical Evidence[a]

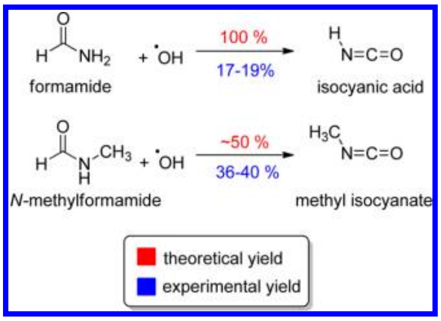

[a]The yields represent the range measured during different experiments.

Methyl isocyanate was detected solely in the oxidation of *N*-methylformamide by OH radicals. This product is of major health concern and was responsible for the death of thousands of residents in Bhopal, India during a methyl isocyanate leak from a nearby pesticide plant in 1984.[33] Methyl isocyanate was previously detected by FTIR from the oxidation of *N*-methylformamide but the product yield was not quantified.[20] In this study, we quantify methyl isocyanate by assuming it has the same sensitivity in the PTR-MS as the average of the amides quantified (17.1 npcs/ppbv; see Table S1).

We employ ab initio calculations to assist in understanding the kinetics of the OH radical reactions with the amides investigated here, as well as the mechanism of isocyanic acid and methyl isocyanate formation. Results are presented for the five amide + OH radical systems, so as to first understand the radical products arising from these reactions and to gain insight into the differences measured in their kinetics. Following this first step, the secondary reactions of key radical products with O_2 are examined, shedding light on the first generation products arising from the photochemical oxidation of these amides.

a. Formamide. Figure 2A shows the oxidative decay of formamide and the production of HNCO. The formamide decay is well captured by the pseudo-first-order fit (red line in Figure 2A). The yield of HNCO was measured to be 17−19% in a set of six reproducible experiments. When fitting the HNCO trace with Equation S8 in a kinetic box model, we find that a yield (γ_2) of 25% best fits the data, similar to the experimental value. Note that HNCO has no appreciable gas-phase loss rate to oxidants within the time frame of these oxidation experiments. Indeed, its ambient temperature lifetime with OH radicals, extrapolated from high-temperature data, is on the order of decades.[34] We consequently do not consider a sink for HNCO when fitting its time trace. To further explore the site of H-abstraction on formamide and the mechanism of HNCO formation from formamide, we turn to ab initio calculations.

In Figure 3, an energy diagram is provided for the formamide + OH radical reaction, where abstraction can take place from either the formyl C−H site (right-hand side, Figure 3) or from the amide N−H site (left-hand side). In both cases, reaction initially proceeds via the formation of a prereaction complex, followed by an H-abstraction transition state that exothermically leads to water and the corresponding $CNOH_2$ radical product. For N−H abstraction, the overall reaction is only mildly exothermic (ca. 3.08 kcal mol^{-1}), reflecting the very high dissociation energy for this bond (116 kcal mol^{-1}). Accordingly, the transition state for N−H abstraction is high in energy, 6.26 kcal mol^{-1} above the reactants, and abstraction from this site will proceed very slowly and is unlikely to contribute in any substantial way to the formamide + OH reaction. The C−H bond in formamide is considerably weaker than the N−H bond (bond dissociation energy of about 93 kcal mol^{-1}), and abstraction at this site is therefore much more facile. Here, the abstraction transition state lies just above the energy of the reactants (0.16 kcal mol^{-1}), and we suggest that this reaction almost exclusively accounts for the formamide + OH products, which would be the NH_2CO radical (+H_2O).

When considering the first generation products for formamide, the NH_2CO radical appears to be the exclusive reaction product, and in the atmosphere it will readily associate with O_2 to yield a peroxyl radical, $NH_2C(O)O_2$. An energy diagram for this reaction is provided in Figure 4. We see that

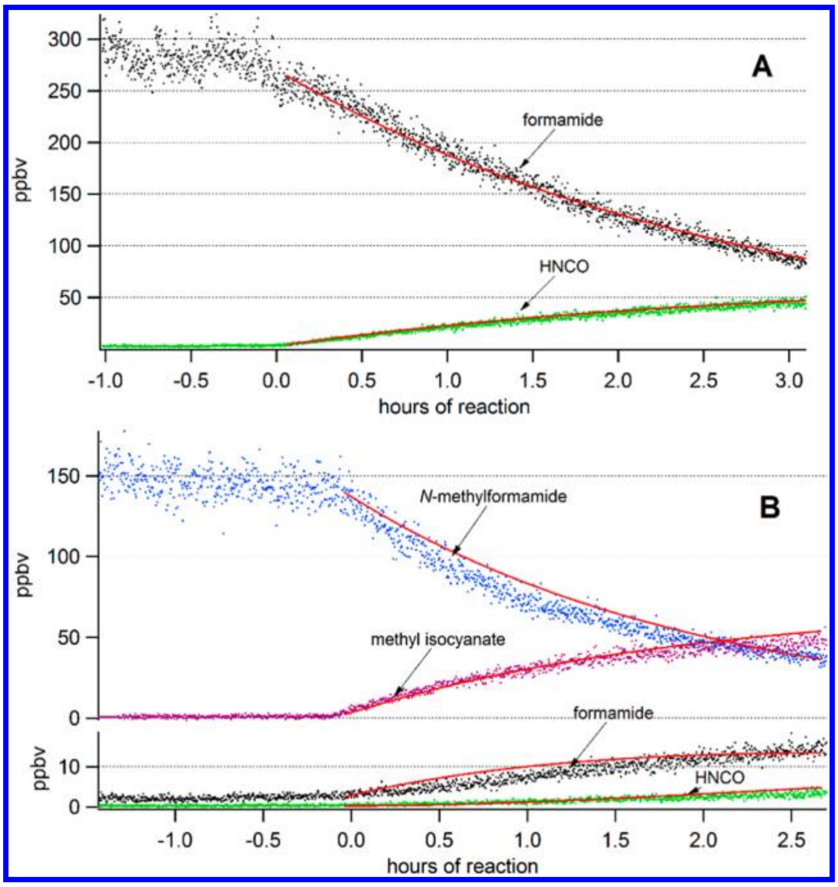

Figure 2. (A) Oxidative decay of formamide and formation of its major primary product, HNCO. The dots represent the 10 s PTR-MS data and the solid red lines represent the exponential fits (Equations S4 and S8 (where $\gamma_2 = 25\%$) for formamide and HNCO, respectively). (B) Oxidative decay of *N*-methylformamide and its products, methyl isocyanate, formamide, and HNCO. The dots represent 10 s PTR-MS data and the solid red lines represent the exponential fits (Equations S4 and S8 (where $\gamma_2 = 50\%$), S6 (where $\gamma_1 = 15\%$), S9 (where $\gamma_1\gamma_2 = 15\%$), for *N*-methylformamide, methyl isocyanate, formamide, and HNCO, respectively).

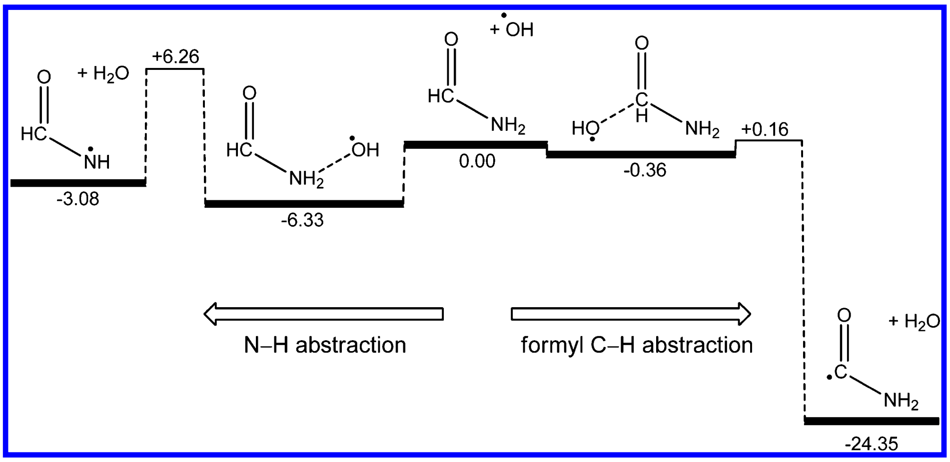

Figure 3. Theoretical energy diagram for formamide + OH. Energies are 0 K enthalpies in kcal mol^{-1}, at the G3X-K level of theory.

O_2 addition to NH_2CO is exothermic by 36.89 kcal mol^{-1}, providing considerable excess vibrational excitation to the peroxyl radical intermediate. Bath gas collisions would be expected to remove this excess energy, providing a thermalized peroxyl radical that could then be lost by bimolecular reactions with NO and other species. Instead, however, the α-amino group provides a low-energy avenue to unimolecular reaction before collisional deactivation can proceed, as recently discovered for α-aminoalkylperoxyl radicals.[35,36] Here, the HO_2 radical is expelled in a concerted process via the transition state shown as an inset in Figure 4. This transition state energy is 19 kcal mol^{-1} above the peroxyl radical and a substantial 17.92 kcal mol^{-1} below the reactants; the vibrationally excited peroxyl radical adduct will initially have more than enough energy to surmount this barrier. Following HO_2 loss, a weak H-bonded adduct is formed, which can dissociate along a barrierless potential to yield isocyanic acid (+HO_2). This process therefore explains the experimental observation of

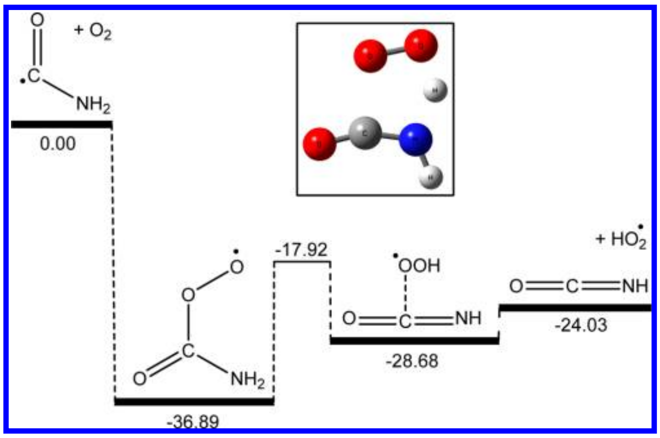

Figure 4. Theoretical energy diagram for formamide's formyl radical + O_2. Energies are 0 K enthalpies in kcal mol^{-1}, at the G3X-K level of theory.

isocyanic acid as the major primary oxidation product of formamide. Based on the reaction energetics and the known chemically activated reaction kinetics of similar peroxyl radicals,[11,37,38] we expect almost quantitative production of HNCO + HO_2 upon reaction of formamide with OH at tropospheric conditions and, therefore, suggest a theoretical yield of 100% (see Scheme 1).

The experimentally measured HNCO yield of 17−19% only accounts for a fraction of the mass balance (Scheme 1). It is therefore possible that surface interactions of HNCO may be affecting its concentration in the gas phase. Perhaps HNCO uptake onto particles or surfaces is also taking place in the chamber. Alternatively, quenching of the $NH_2C(O)O_2$ radical could be an appreciable process, in which case bimolecular chemistry is expected to lead to the carbonyloxyl radical $NH_2C(O)O$, which would likely dissociate rapidly to CO_2 and the aminyl radical NH_2.[39] Further investigation of HNCO's heterogeneous chemistry is currently ongoing in our laboratory to address this discrepancy.

b. N-Methylformamide. The progress of the reaction of *N*-methylformamide with OH radicals is illustrated in Figure 2B. Methyl isocyanate appears to be the major product and was measured in 36−40% yield. The fit using Equation S8 with a γ_2 = 50% seems to reproduce the data well. The fit for methyl isocyanate in Figure 2B does not consider any sink terms, as its reactivity toward OH radicals is estimated to be ~10^{-13} cm^3 molec^{-1} s^{-1} by the EPI Suite model and would account for <1% difference in the fit.[40] Formamide (fit of 15%) and HNCO were also detected as oxidation products (Figure 2B). Note that in Figure 2B, HNCO is treated as a secondary product arising solely from the oxidation of formamide (Equation S9).

Figure 5 depicts a theoretical energy diagram for the *N*-methylformamide reaction with OH, proceeding via abstraction at either of the two unique C−H sites. Abstraction of an N−H hydrogen is again energetically uncompetitive (with transition state 4.03 kcal mol^{-1} above the reactants) and is shown only in the Supporting Information (Figure S6). We observe in Figure 5 that the OH radical can abstract a H atom from either carbon, leading to the CH_2NHCHO (left-hand side) or CH_3NHCO (right-hand side) radicals. In both cases, the transition states lie below the reactants in energy, at −1.30 kcal mol^{-1} and −0.67 kcal mol^{-1}, for the respective alkyl and formyl abstractions. This result is consistent with the rate coefficient of *N*-methylformamide being more than twice that of formamide. Considering the uncertainty of the calculations reported here, we cannot definitively discriminate between the CH_2NHCHO and the CH_3NHCO radical products. As such, we assign theoretical yields of 50% to both products as a rough initial estimate (see Scheme 1).

Energy diagrams for the reaction of O_2 with the respective CH_2NHCHO and CH_3NHCO radicals are shown in Figure 6. For the CH_2NHCHO radical (top of Figure 6), the resultant peroxyl radical can eliminate HO_2 to yield an imine, but the required barrier heights are at around the energy of the entrance channel, and the initially excited peroxyl radical will be rapidly deactivated to below the required thresholds. Interestingly, the high barrier for this process arises from the reaction thermodynamics, with the conjugated imine product CH_2NCHO being comparatively unfavorable. Note also from Figure 6 that an intramolecular abstraction from the formyl group can take place, at 4.44 kcal mol^{-1} below the reactants, forming a radical intermediate that can ultimately dissociate to HNCO and CH_2OOH (although again at above the reactant energy). Indeed, HNCO was detected experimentally in <5% yield, and may have two gas phase sources within these experiments: a primary product from the reaction of CH_2NHCHO + OH (as discussed above) and a secondary

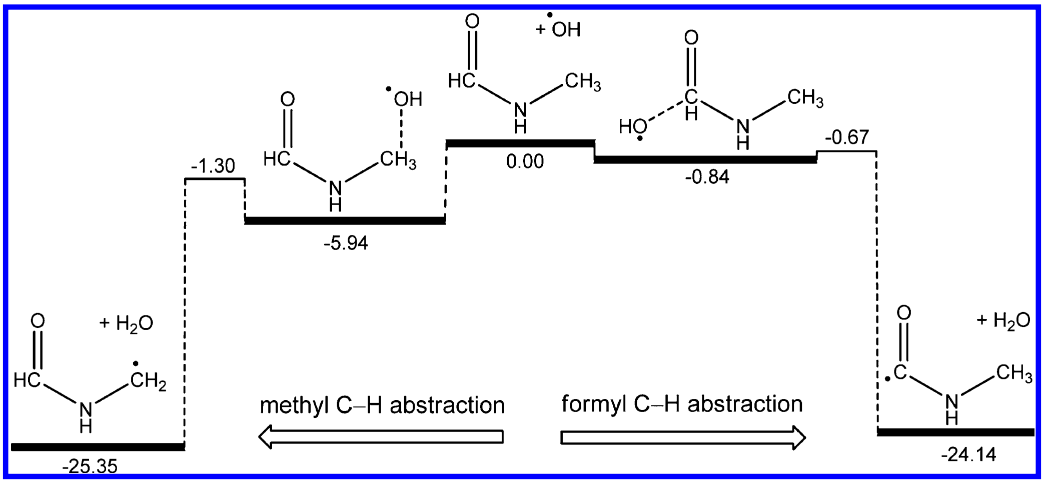

Figure 5. Theoretical energy diagram for *N*-methylformamide + OH. Energies are 0 K enthalpies in kcal mol^{-1}, at the G3X-K level of theory. The N−H abstraction requires a significant barrier (4.03 kcal mol^{-1}) and is shown in Figure S6.

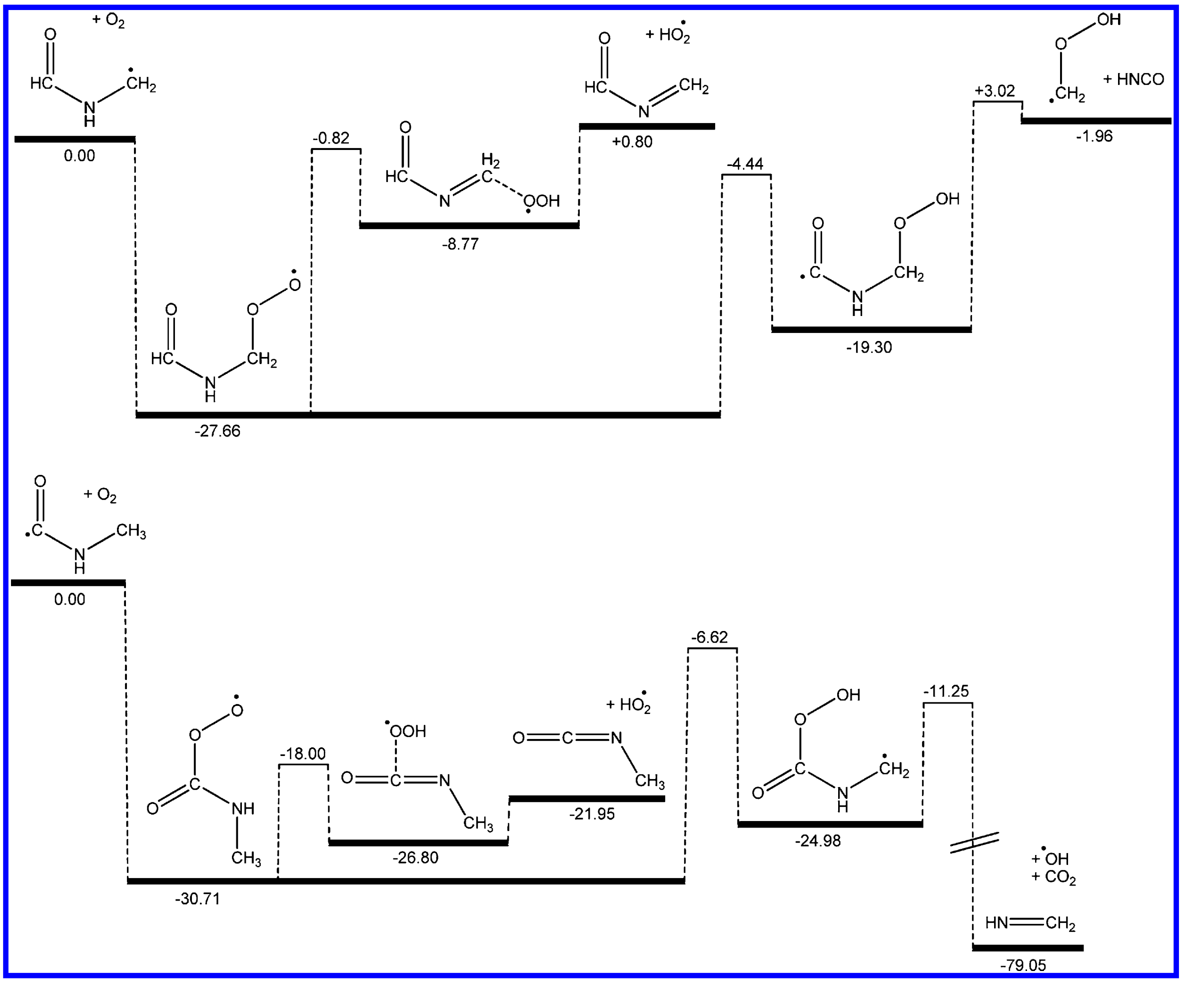

Figure 6. Theoretical energy diagrams for *N*-methylformamide's methyl radical + O_2 (top) and formyl radical + O_2 (bottom) reactions. Energies are 0 K enthalpies in kcal mol^{-1}, at the G3X-K level of theory.

product from the oxidation of formamide, which was also detected in the oxidation of *N*-methylformamide.

According to our theoretical results, the O_2CH_2NHCHO peroxyl radical can be collisionally deactivated under tropospheric conditions, allowing it to be removed through bimolecular chemistry (Scheme S1). If this peroxyl radical is converted to the corresponding alkoxyl radical, OCH_2NHCHO, through reaction with NO (and other radicals), *β*-scission at the C−N bond could then lead to formaldehyde and the NHCHO radical, whereas C−H scission (or H abstraction by O_2) would yield $NH(CHO)_2$, diformamide (Scheme S1). The NHCHO aminyl radical formation is of interest as they are generally thought to be removed from the atmosphere through reaction with radical species such as NO and NO_2, potentially leading to toxic compounds that include nitrosamines and nitramines.[9] If the NHCHO aminyl radical is formed in the *N*-methylformamide chamber experiments, it could be long-lived enough to abstract a H from another compound in the chamber and produce formamide, which was detected as an oxidation product, albeit with low yields (<30%). However, the production of formamide in these oxidation experiments does not show purely first order kinetics, underlining the possibility that heterogeneous chemistry may also be occurring on the chamber walls (Figure 2B). On the other hand, Barnes et al. detected diformamide as an oxidation of *N*-methylformamide in an estimated 50% yield.[20] In our oxidation experiments, the diformamide protonated molecular ion (*m*/*z* 74) was detected by the PTR-MS but as a trace product with signal intensities consistently less than the signal of HNCO (see Figure 2B), and so we did not quantify its yield.

Upon reaction of the CH_3NHCO radical with O_2, a facile unimolecular reaction pathway is available, as illustrated in the bottom half of Figure 6. Similar to the formamide NH_2CO radical, O_2 addition produces a peroxyl radical that can eliminate HO_2 via a barrier 18.00 kcal mol^{-1} below the reactants. This reaction leads to the experimentally observed reaction product methyl isocyanate. A second mechanism that also proceeds with a transition state energy below the reactants is available with a relative barrier height of −6.62 kcal mol^{-1}. In this case, the peroxyl group abstracts an H atom from the *N*-methyl moiety, ultimately yielding CH_2NH and CO_2 and regenerating the OH radical in the process. This mechanism has been identified in secondary and tertiary amines and is known to be uncompetitive with the facile HO_2 elimination reaction, when available.[41] The experimental methyl isocyanate yield of 36−40% is commensurate with similar yields of both CH_2NHCHO and CH_3NHCO evolving from the reaction of OH radicals with *N*-methylformamide, followed by almost quantitative conversion of CH_3NHCO to CH_3NCO + HO_2. These results are also consistent with methyl isocyanate detected by Barnes et al. from the oxidation of *N*-methylformamide.[20]

c. Acetamide. Acetamide reacted away too slowly within our experimental setup to analyze its products. We show through ab initio calculations that acetamide is indeed expected to react more slowly than the other amides considered in this study. A theoretical energy diagram for the acetamide + OH reaction is provided in Figure S7. Here, an H-abstraction can again transpire at the nitrogen, but with a barrier significantly above the reactant energies (>5 kcal mol^{-1}), and this process is expected to be negligible. Instead, abstraction from the methyl group is thought to dominate, proceeding via a transition state at 2.04 kcal mol^{-1} above the reactants, leading to the $CH_2C(O)NH_2$ radical as the major product. The relatively large barrier for this reaction can explain the slow kinetics reported here, where the rate coefficient is measured to be a fraction of that of the formamide + OH reaction. The slow rate of reaction also likely contributes to the difficulties associated with obtaining reproducible measurements of the acetamide + OH rate coefficient in the chamber experiments. According to these calculations, the N−H abstraction is uncompetitive, in contrast to the proposed mechanism by Barnes et al.,[20] and we therefore suggest that the abstraction occurs solely on the methyl group. The products have yet to be quantified, although we did detect formamide and HNCO, but we believe that the proposed 100% yield for HNCO by Barnes et al. is unlikely.[20]

d. N-Methylacetamide. Time traces of the evolution of the products of *N*-methylacetamide are presented in Figure S4. Formamide was detected as the major product with measured yields between 62 and 87% and a fit of 80% yield best reproduced its experimental trace. A product at m/z 60 was also observed and could be either *N*-methylformamide or acetamide. Its trace was fitted with a yield of 10% using Equation S6 under the assumption that m/z 60 is a primary product but has a sink with a rate coefficient similar to acetamide's with OH. HNCO was also detected as a product and was fitted with Equation S9.

A theoretical energy diagram for *N*-methylacetamide's reaction with OH is provided as Figure S8. The ab initio calculations once again indicate that abstraction from the N−H site requires a large barrier (3.35 kcal mol^{-1}) and it is not discussed further. There are two unique C−H bonds in *N*-methylacetamide, analogous to the respective methyl group abstractions in acetamide and in *N*-methylformamide. The lowest barrier to reaction corresponds to H atom abstraction from the *N*-methyl group, producing the $CH_2NHC(O)CH_3$ radical. This radical should be the dominant reaction product, accompanied by lesser quantities of $CH_3NHC(O)CH_2$. The calculated overall barrier height for *N*-methyl H-abstraction (−1.96 kcal mol^{-1}) is similar to, but somewhat less than, the equivalent H-abstraction in *N*-methyformamide (−1.30 kcal mol^{-1}) due to the introduction of the acetyl functional group. The substantially higher experimental rate coefficient for the *N*-methylformamide versus *N*-methylacetamide reaction with OH therefore provides further support for our finding that formyl C−H abstractions are primary processes in the photochemical oxidation of amides, when available. The barrier for H-abstraction from the acetyl group in *N*-methylacetamide (1.34 kcal mol^{-1}) is also reduced somewhat from that for the analogous process in acetamide (2.04 kcal mol^{-1}) by introduction of the *N*-methyl substituent, although it remains above the reactant energies.

Formamide may arise as a secondary oxidation product of the $CH_2NHC(O)CH_3$ radical (by analogy to *N*-methylformamide). Since this radical is the major reaction product, it may be consistent with formamide yields in the range of 62−87%. Formamide may also be produced as an oxidation product of *N*-methylacetamide originating from the $CH_3NHC(O)CH_2$ radical. We also cannot rule out the possibility that formamide is being produced via heterogeneous chemistry occurring on the walls of the chamber and the exact mechanism of formamide production remains unclear. Comparatively, Barnes et al. state that they were unable to detect formamide in their experimental setup due to interferences with the OH radical precursor, CH_3ONO, and potential oxidation products.[20]

e. Propanamide. Time traces of the evolution of the products of propanamide are presented in Figure S5. The major oxidation product detected is formamide but its experimentally measured yield fell within the uncertainty associated with the formamide production during amide-free control experiments so we only report a < 30% yield. On the other hand, using Equation S6 in a kinetic box model to fit the formamide trace, we obtain a yield of 60%. The discrepancy between the measured and fitted yields is likely due to the presence of a sink for formamide at long reaction times (see Figure S5). HNCO was detected during the experimental oxidation and again may be a primary or secondary product.

When the methyl group in acetamide is extended to an ethyl group, as in the case of propanamide, we find that N−H abstraction still requires a significant barrier, but that abstraction from the now secondary C−H carbon has a slightly lower (but still positive) transition state barrier of +0.34 kcal mol^{-1} (Figure S9). On the other hand, abstraction from the primary C−H site proceeds with a barrier just below the reactants (−0.30 kcal mol^{-1}). Within the accuracy of the reported calculations, we therefore suggest that both the $CH_2CH_2C(O)NH_2$ and $CH_3CHC(O)NH_2$ radicals will arise as products of the propanamide + OH reaction. These results also support a rate coefficient for the reaction of propanamide with OH that is toward the lower end of the amides measured in this study.

Even though we are not quantitative about the yield of formamide from the oxidation of propanamide, its production could originate from the minor $NH_2C(O)CHCH_3$ radical product, relative to the $NH_2C(O)CH_2CH_2$ radical (which we then hypothesize cannot lead to formamide production). Irrespective of these speculations, the specific pathways that result in relatively high yields of formamide from oxidation of all of the substituted amides studied here remain to be resolved and the role of heterogeneous chemistry should also be considered.

3. Reactivity Trends. Figure 7 provides the structures of nine simple amides and includes a summary of the rate coefficients measured in this work and in previous work. The compounds are arranged in rows with increasing degree of *N*-methylation from left to right, and in columns with increasing length of alkyl chain from top to bottom. The rate coefficients increase as a function of increasing number of methyl groups on the nitrogen. This observation may be explained by the addition of a methyl group which adds a competitive reactive pathway for H-abstraction from the methyl C−H. Yet, the ability of the methyl group to donate electron density to the amide bond facilitates the H-abstraction of the acetyl C−H by the electrophilic OH radical. There is a decreasing reactivity trend from formamide to propanamide to acetamide toward

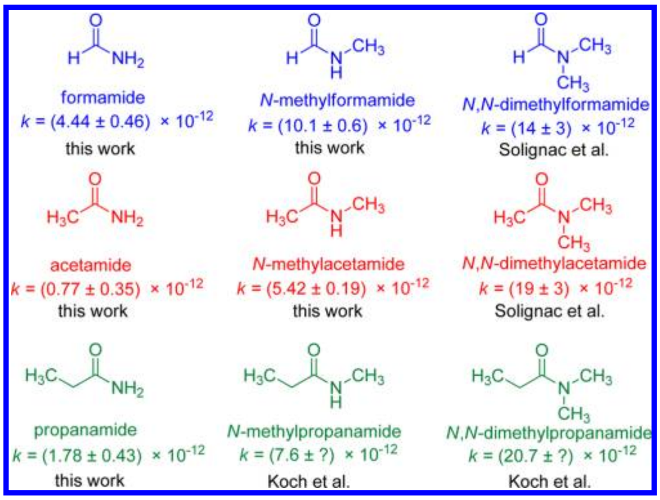

Figure 7. Summary of room temperature rate coefficients with OH radicals of nine amides based on their alkyl chain length (grouped by colors) and degree of *N*-methylation (grouped by column).

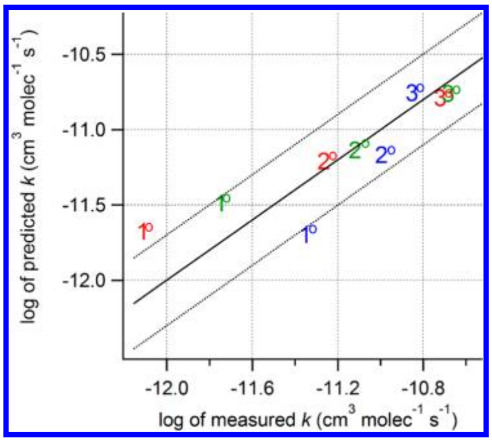

Figure 8. Plot of predicted rate coefficients using EPA's EPI Suite model as a function of experimentally measured rate coefficients for the nine amides in Figure 7. The numbers represent the level of *N*-methylation on the amide, so that 1° represents primary amides, 2° represents secondary amides, and 3° represents tertiary amides. The color coding matches Figure 7 so that the blue series represents formamide and its alkylated analogues, the red series represents acetamide and its alkylated analogues, and the green series represents propanamide and its alkylated analogues. The solid line is the 1:1 relationship, and the dotted lines have slopes differing by a factor of 2 from the 1:1 relationship.

OH radicals which also seems to hold true for their methylated analogues. This trend is not straightforward since the H-abstraction occurs at different locations on the H/alkyl functional group attached to the carbonyl, dictating the preferred mechanistic pathway and hence influencing the experimental rate coefficient.

The rate coefficients of amides with OH radicals are slower than with their homologous amine. For example, the rate coefficient of methylamine, the homologue of formamide has a rate coefficient of $(17.3 \pm 1.1) \times 10^{-12}$ cm^3 molec^{-1} s^{-1}, almost four times the rate of formamide.[42] The carbonyl moiety draws electron density from the functional groups on either side of its carbon atom, rendering them less reactive toward an OH radical. This chemical property explains why amides are longer lived in the atmosphere than amines. An incomplete homologous summary for amines is depicted in Figure S10.

The U.S. Environmental Protection Agency's (EPA) Estimation Program Interface (EPI) Suite model was used to compare the experimentally determined amide rate coefficients shown in Figure 7 with their empirical estimates.[40] The AOPWIN module (v1.92) within the EPI suite model employs structure−activity relationships (SARs) for estimating OH reaction rate coefficients based on those developed by Atkinson and co-workers.[28,43,44] Figure 8 shows the correlation between the predicted rate coefficients using EPI Suite and the measured rate coefficients; the numbers (1°, 2°, 3°) represent the degree of *N*-methylation on the amide, and the colors match the amide groups in Figure 7. The model appears to correctly predict the influence of the changing degree of *N*-methylation, but struggles to represent the primary amides (formamide, acetamide, and propanamide). These primary amides are the slowest to react with OH and, consequently, have the longest atmospheric lifetimes.

Upon consultation of the AOPWIN user guide, we can better assess the origin of the predicted rate coefficients. Interestingly, the AOPWIN model does not consider formyl C−H abstractions in amides, but does include N−H abstractions, along with reaction at saturated carbon atoms (see Supporting Information for relevant AOPWIN notes). However, our ab initio and product detection results demonstrate that the formyl C−H and the alpha C−H abstractions are likely to be major reaction channels for the amides. Furthermore, we show that N−H abstractions, when available, should in all cases be negligible. Attempts to determine a value for the substituent factor $F(-C(O)N<)$ for amides in the context of the SAR model of Kwok and Atkinson[44] proved to be difficult with the limited data set of rate coefficients presently available, and further kinetic studies are needed. However, our experiments on formamide suggest that the rate coefficient term $k(HC(O)N<)$ should be around 4×10^{-12} cm^3 molec^{-1} s^{-1} and this number is also compatible with the available data for *N*-methyl and *N*,*N*-dimethylformamide. In comparison, the analogous aldehyde C−H abstraction rate coefficient term is 17×10^{-12} cm^3 molec^{-1} s^{-1}.[44] It is therefore apparent that the $-NH_2$ group is deactivating the formyl C−H abstraction, although not to the extent where it can be neglected altogether (as is presently the case). The rate coefficient component attributable to *N*-methyl abstractions should be about 5×10^{-12} cm^3 molec^{-1} s^{-1}, consistent with most of the reactivity occurring on the methyl group for *N*-methylacetamide for example. Furthermore, a total rate coefficient on the order of 10×10^{-12} cm^3 molec^{-1} s^{-1} for *N*-methylformamide agrees well with the reaction proceeding at almost equivalent rates at the alkyl and formyl substituents. It does appear that *N*-methylation of amides has a minor impact upon the reactivity of the acetyl functionality, and vice versa.

This analysis prompted us to consider the analogous series of amines shown in Figure S10, and their predicted rate coefficients are plotted against the experimentally measured rate coefficients of amines with OH radicals in Figure S11. The AOPWIN output predicts a major contribution from the N−H abstraction mechanism. Nonetheless, the N−H abstraction channel appears to be of more significance for amines than for amides.[11,45] This study's mechanistic work suggests a reevaluation of the way that H-abstraction is treated for organo-nitrogen compounds within the AOPWIN model and ongoing work in our laboratory aims to address this issue.

■ CONCLUSIONS

The rate coefficients of the oxidation of five different amides with OH radicals were measured for formamide (4.44 ± 0.46) $\times 10^{-12}$ cm^3 molec^{-1} s^{-1}, *N*-methylformamide (10.1 ± 0.6) $\times 10^{-12}$ cm^3 molec^{-1} s^{-1}, acetamide (0.4−1.1) $\times 10^{-12}$ cm^3 molec^{-1} s^{-1}, *N*-methylacetamide (5.42 ± 0.19) $\times 10^{-12}$ cm^3 molec^{-1} s^{-1}, and propanamide (1.78 ± 0.43) $\times 10^{-12}$ cm^3 molec^{-1} s^{-1} using relative rate experiments in a 1 m^3 smog chamber. These rate coefficients correspond to a wide range of lifetimes against OH radicals on the order of 0.5−7 days using an OH radical concentration of 2×10^6 molecules cm^{-3}. It is therefore likely that reactions with OH radicals are the dominant daytime sink for amides.

The evolution of the amides was monitored by PTR-MS and so was the production of *N*-containing products, which included toxic gas-phase molecules like HNCO and methyl isocyanate. The time trace of the oxidation products were also modeled using kinetic equations. The ab initio calculations presented can explain the observation of HNCO and CH_3NCO upon the reaction of formamide and *N*-methylformamide, respectively, with OH radicals. The peroxyl radical mechanisms developed here are also consistent with no direct isocyanate formation from any of the other amides investigated in this study (although other isocyanates could be reasonably expected to form in the OH radical reactions of other *N*-substituted derivatives of formamide). The mechanism for formamide production from *N*-methyl formamide and the other substituted amides, however, remains unclear. Furthermore, we expect that reactions with NO_3 radicals or Cl radicals would lead to similar mechanistic pathway assuming a H-abstraction mechanism.

■ ASSOCIATED CONTENT

Ⓢ Supporting Information

Further details on the experimental setup and HNCO calibration are described. Experimental and theoretical details of acetamide, *N*-methylacetamide, and propanamide are also included. This material is available free of charge via the Internet at http://pubs.acs.org.

■ AUTHOR INFORMATION

Corresponding Authors

*E-mail: jmurphy@chem.utoronto.ca.
*E-mail: jabbatt@chem.utoronto.ca.

Notes

The authors declare no competing financial interest.

■ ACKNOWLEDGMENTS

The authors acknowledge the Canada Foundation for Innovation and the Ontario Research Fund for infrastructure support and NSERC and Environment Canada for operational support. N.B. would like to thank Vanier Canada Graduate Scholarships for funding. G.d.S. is grateful for support through the Australian Research Council (DP110103889, DP130100862, FT130101304). The authors would also like to thank John Liggio for donating the HNCO source, as well as Gregory Wentworth for help with the ion chromatograph.

■ REFERENCES

(1) Ge, X.; Wexler, A. S.; Clegg, S. L. Atmospheric Amines - Part I. A Review. *Atmos. Environ.* **2011**, *45*, 524−546.

(2) Schmeltz, I.; Hoffmann, D. Nitrogen-Containing Compounds in Tobacco and Tobacco Smoke. *Chem. Rev.* **1977**, *77*, 295−311.

(3) Leach, J.; Blanch, A.; Bianchi, A. C. Volatile Organic Compounds in an Urban Airborne Environment Adjacent to a Municipal Incinerator, Waste Collection Centre and Sewage Treatment Plant. *Atmos. Environ.* **1999**, *33*, 4309−4325.

(4) Rogge, W. F.; Hildemann, L. M.; Mazurek, M. A.; Cass, G. R.; Simoneit, B. R. T. Sources of Fine Organic Aerosol. 1. Charbroilers and Meat Cooking Operations. *Environ. Sci. Technol.* **1991**, *25*, 1112−1125.

(5) Sollinger, S.; Levsen, K.; Wünsch, G. Indoor Pollution by Organic Emissions from Textile Floor Coverings: Climate Test Chamber Studies Under Static Conditions. *Atmos. Environ.* **1994**, *28*, 2369−2378.

(6) Cheng, Y.; Li, S.; Leithead, A. Chemical Characteristics and Origins of Nitrogen-Containing Organic Compounds in PM2.5 Aerosols in the Lower Fraser Valley. *Environ. Sci. Technol.* **2006**, *40*, 5846−5852.

(7) Laskin, A.; Smith, J. S.; Laskin, J. Molecular Characterization of Nitrogen-Containing Organic Compounds in Biomass Burning Aerosols Using High-Resolution Mass Spectrometry. *Environ. Sci. Technol.* **2009**, *43*, 3764−3771.

(8) Raja, S.; Raghunathan, R.; Kommalapati, R. R.; Shen, X.; Collett, J. L., Jr.; Valsaraj, K. T. Organic Composition of Fogwater in the Texas−Louisiana Gulf Coast Corridor. *Atmos. Environ.* **2009**, *43*, 4214−4222.

(9) Nielsen, C. J.; Herrmann, H.; Weller, C. Atmospheric Chemistry and Environmental Impact of the Use of Amines in Carbon Capture and Storage (CCS). *Chem. Soc. Rev.* **2012**, 6684−6704.

(10) Zhu, L.; Schade, G. W.; Nielsen, C. J. Real-Time Monitoring of Emissions from Monoethanolamine-Based Industrial Scale Carbon Capture Facilities. *Environ. Sci. Technol.* **2013**, *47*, 14306−14314.

(11) da Silva, G. Atmospheric Chemistry of 2-Aminoethanol (MEA): Reaction of the NH_2CHCH_2OH Radical with O_2. *J. Phys. Chem. A* **2012**, *116*, 10980−10986.

(12) Xie, H.; Li, C.; He, N.; Wang, C.; Zhang, S.; Chen, J. Atmospheric Chemical Reactions of Monoethanolamine Initiated by OH Radical: Mechanistic and Kinetic Study. *Environ. Sci. Technol.* **2014**, *48*, 1700−1706.

(13) Chakir, A.; Solignac, G.; Mellouki, A.; Daumont, D.; Gas Phase, U. V. Absorption Cross-Sections for a Series of Amides. *Chem. Phys. Lett.* **2005**, *404*, 74−78.

(14) Koch, R.; Palm, W. -.; Zetzsch, C. First Rate Constants for Reactions of OH Radicals with Amides. *Int. J. Chem. Kinet.* **1997**, *29*, 81−87.

(15) Aschmann, S. M.; Atkinson, R. Atmospheric Chemistry of 1-Methyl-2-pyrrolidinone. *Atmos. Environ.* **1999**, *33*, 591−599.

(16) Muñoz, A.; Vera, T.; Sidebottom, H.; Ródenas, M.; Borrás, E.; Vázquez, M.; Raro, M.; Mellouki, A. Studies on the Atmospheric Fate of Propachlor (2-Chloro-*N*-isopropylacetanilide) in the Gas-Phase. *Atmos. Environ.* **2012**, *49*, 33−40.

(17) Jackson, D. A.; Wallington, T. J.; Mabury, S. A. Atmospheric Oxidation of Polyfluorinated Amides: Historical Source of Perfluorinated Carboxylic Acids to the Environment. *Environ. Sci. Technol.* **2013**, *47*, 4317−4324.

(18) Solignac, G.; Mellouki, A.; Le Bras, G.; Barnes, I.; Benter, T. Kinetics of the OH and Cl Reactions with N-Methylformamide, *N,N*-Dimethylformamide and *N,N*-Dimethylacetamide. *J. Photochem. Photobiol., A* **2005**, *176*, 136−142.

(19) Solignac, G.; Magneron, I.; Mellouki, A.; Muñoz, A.; Reviejo, M. M.; Wirtz, K. A Study of the Reaction of OH Radicals with N-Methyl Pyrrolidinone, N-Methyl Succinimide and N-Formyl Pyrrolidinone. *J. Atmos. Chem.* **2006**, *54*, 89−102.

(20) Barnes, I.; Solignac, G.; Mellouki, A.; Becker, K. H. Aspects of the Atmospheric Chemistry of Amides. *ChemPhysChem* **2010**, *11*, 3844−3857.

(21) El Dib, G.; Chakir, A. Temperature-Dependence Study of the Gas-Phase Reactions of Atmospheric NO_3 Radicals with a Series of Amides. *Atmos. Environ.* **2007**, *41*, 5887−5896.

(22) Borduas, N.; Abbatt, J. P. D.; Murphy, J. G. Gas Phase Oxidation of Monoethanolamine (MEA) with OH Radical and Ozone: Kinetics, Products, and Particles. *Environ. Sci. Technol.* **2013**, *47*, 6377−6383.

(23) De Gouw, J.; Warneke, C. Measurements of Volatile Organic Compounds in the Earth's Atmosphere Using Proton-Transfer-Reaction Mass Spectrometry. *Mass Spectrom. Rev.* **2007**, *26*, 223−257.

(24) Gylestam, D.; Karlsson, D.; Dalene, M.; Skarping, G. Determination of Gas Phase Isocyanates Using Proton Transfer Reaction Mass Spectrometry. *Anal. Chem. Lett.* **2011**, *1*, 261−271.

(25) Zhao, Y.; Truhlar, D. The M06 Suite of Density Functionals for Main Group Thermochemistry, Thermochemical Kinetics, Noncovalent Interactions, Excited States, and Transition Elements: Two New Functionals and Systematic Testing of Four M06-Class Functionals and 12 Other Functionals. *Theor. Chem. Acc.* **2008**, *120*, 215−241.

(26) da Silva, G. G3X-K Theory: A Composite Theoretical Method for Thermochemical Kinetics. *Chem. Phys. Lett.* **2013**, *558*, 109−113.

(27) Frisch, M. J.; Trucks, G. W.; Schlegel, H. B.; Scuseria, G. E.; Robb, M. A.; Cheeseman, J. R.; Montgomery, J. J. A.; Vreven, T.; Kudin, K. N.; Burant, J. C. et al. *Gaussian 09*, revision B.01; Gaussian, Inc.: Wallingford, CT, 2010.

(28) Atkinson, R. Kinetics and Mechanisms of the Gas-Phase Reactions of the Hydroxyl Radical with Organic Compounds Under Atmospheric Conditions. *Chem. Rev.* **1986**, *86*, 69−201.

(29) Hurley, M. D.; Wallington, T. J.; Laursen, L.; Javadi, M. S.; Nielsen, O. J.; Yamanaka, T.; Kawasaki, M. Atmospheric Chemistry of n-Butanol: Kinetics, Mechanisms, and Products of Cl Atom and OH Radical Initiated Oxidation in the Presence and Absence of NO_x. *J. Phys. Chem. A* **2009**, *113*, 7011−7020.

(30) Roberts, J. M.; Veres, P. R.; Cochran, A. K.; Warneke, C.; Burling, I. R.; Yokelson, R. J.; Lerner, B.; Gilman, J. B.; Kuster, W. C.; Fall, R.; de Gouw, J. Isocyanic Acid in the Atmosphere and Its Possible Link to Smoke-Related Health Effects. *Proc. Natl. Acad. Sci. U.S.A.* **2011**, *108*, 8966−8971.

(31) Wentzell, J. J. B.; Liggio, J.; Li, S.; Vlasenko, A.; Staebler, R.; Lu, G.; Poitras, M.; Chan, T.; Brook, J. R. Measurements of Gas Phase Acids in Diesel Exhaust: A Relevant Source of HNCO? *Environ. Sci. Technol.* **2013**, *47*, 7663−7671.

(32) Roberts, J. M.; Veres, P. R.; VandenBoer, T. C.; Warneke, C.; Graus, M.; Williams, E. J.; Lefer, B.; Brock, C. A.; Bahreini, R.; Öztürk, F.; Middlebrook, A. M.; Wagner, N. L.; Dubé, W. P.; de Gouw, J. A. New Insights into Atmospheric Sources and Sinks of Isocyanic Acid, HNCO, from Recent Urban and Regional Observations. *J. Geophys. Res. Atmos.* **2014**, DOI: 2013JD019931.

(33) Broughton, E. The Bhopal Disaster and its Aftermath: A Review. *Environ. Health* **2005**, *4*, 6.

(34) Tsang, W. Chemical Kinetic Data Base for Propellant Combustion. II. Reactions Involving CN, NCO, and HNCO. *J. Phys. Chem. Ref. Data* **1992**, *21*, 753−791.

(35) Ly, T.; Kirk, B. B.; Hettiarachchi, P. I.; Poad, B. L. J.; Trevitt, A. J.; da Silva, G.; Blanksby, S. J. Reactions of Simple and Peptidic Alpha-Carboxylate Radical Anions with Dioxygen in the Gas Phase. *Phys. Chem. Chem. Phys.* **2011**, *13*, 16314−16323.

(36) da Silva, G.; Kirk, B. B.; Lloyd, C.; Trevitt, A. J.; Blanksby, S. J. Concerted HO_2 Elimination from α-Aminoalkylperoxyl Free Radicals: Experimental and Theoretical Evidence from the Gas-Phase $NH_2^{\bullet}CHCO_2^- + O_2$ Reaction. *J. Phys. Chem. Lett.* **2012**, *3*, 805−811.

(37) da Silva, G.; Bozzelli, J. W.; Liang, L.; Farrell, J. T. Ethanol Oxidation: Kinetics of the α-Hydroxyethyl Radical + O_2 Reaction. *J. Phys. Chem. A* **2009**, *113*, 8923−8933.

(38) Rissanen, M. P.; Eskola, A. J.; Nguyen, T. L.; Barker, J. R.; Liu, J.; Liu, J.; Halme, E.; Timonen, R. S. $CH_2NH_2 + O_2$ and $CH_3CHNH_2 + O_2$ Reaction Kinetics: Photoionization Mass Spectrometry Experiments and Master Equation Calculations. *J. Phys. Chem. A* **2014**, *118*, 2176−2186.

(39) Poad, B. L. J.; Kirk, B. B.; Hettiarachchi, P. I.; Trevitt, A. J.; Blanksby, S. J.; Clark, T. Direct Detection of a Persistent Carbonyloxyl Radical in the Gas Phase. *Angew. Chem., Int. Ed.* **2013**, *52*, 9301−9304.

(40) *U.S. EPA Estimation Programs Interface Suite for Microsoft Windows*, version 4.11.; 2014.

(41) Onel, L.; Thonger, L.; Blitz, M. A.; Seakins, P. W.; Bunkan, A. J. C.; Solimannejad, M.; Nielsen, C. J. Gas-Phase Reactions of OH with Methyl Amines in the Presence or Absence of Molecular Oxygen. An Experimental and Theoretical Study. *J. Phys. Chem. A* **2013**, *117*, 10736−10745.

(42) Carl, S. A.; Crowley, J. N. Sequential Two (Blue) Photon Absorption by NO_2 in the Presence of H_2 as a Source of OH in Pulsed Photolysis Kinetic Studies: Rate Constants for Reaction of OH with CH_3NH_2, $(CH_3)_2NH$, $(CH_3)_3N$, and $C_2H_5NH_2$ at 295 K. *J. Phys. Chem. A* **1998**, *102*, 8131−8141.

(43) Atkinson, R. A Structure-Activity Relationship for the Estimation of Rate Constants for the Gas-Phase Reactions of OH Radicals with Organic Compounds. *Int. J. Chem. Kinet.* **1987**, *19*, 799−828.

(44) Kwok, E. S. C.; Atkinson, R. Estimation of Hydroxyl Radical Reaction Rate Constants for Gas-Phase Organic Compounds Using a Structure-Reactivity Relationship: An Update. *Atmos. Environ.* **1995**, *29*, 1685−1695.

(45) Galano, A.; Alvarez-Idaboy, J. Branching Ratios of Aliphatic Amines + OH Gas-Phase Reactions: A Variational Transition-State Theory Study. *J. Chem. Theory Comput.* **2008**, *4*, 322−327.